J. Fluid Mech. (1985), *vol.* 157, *pp.* 17–33
Printed in Great Britain

Transient axisymmetric motion of a floating cylinder

By J. N. NEWMAN

Department of Ocean Engineering, Massachusetts Institute of Technology,
Cambridge, Massachusetts 02139

(Received 15 June 1984 and in revised form 14 January 1985)

A linear theory is developed in the time domain for vertical motions of an axisymmetric cylinder floating in the free surface. The velocity potential is obtained numerically from a discretized boundary-integral-equation on the body surface, using a Galerkin method. The solution proceeds in time steps, but the coefficient matrix is identical at each step and can be inverted at the outset.

Free-surface effects are absent in the limits of zero and infinite time. The added mass is determined in both cases for a broad range of cylinder depths. For a semi-infinite cylinder the added mass is obtained by extrapolation.

An impulse-response function is used to describe the free-surface effects in the time domain. An oscillatory error observed for small cylinder depths is related to the irregular frequencies of the solution in the frequency domain. Fourier transforms of the impulse-response function are compared with direct computations of the damping and added-mass coefficients in the frequency domain. The impulse-response function is also used to compute the free motion of an unrestrained cylinder, following an initial displacement or acceleration.

1. Introduction

If a floating body performs unsteady motions of small amplitude, the linearized hydrodynamic pressure force exerted on the fluid can be analysed either in the time or the frequency domain. The latter, which usually is employed, corresponds to a physical situation where the motions of the body and surrounding fluid are harmonic in time. In this case the dynamic pressure force due to the motions of the body can be expressed as a linear function of its velocity and acceleration, with the respective coefficients known as the damping and added mass. Both coefficients are frequency dependent. Numerous computational studies have been performed in the frequency domain to determine these coefficients for specific two- and three-dimensional bodies.

The linear analysis for the analogous time-domain problem is described by Wehausen (1971), but few computations have been made directly from this basis. A canonical body motion can be assumed, such as a step-function velocity and delta-function acceleration. In this case the subsequent time-varying force exerted by the body on the surrounding fluid is known as the impulse-response function. Since free-surface effects persist indefinitely in an inviscid fluid, the impulse-response function has the same property.

Another type of transient problem may be defined, where the body is given an initial disturbance from equilibrium, and subsequently responds freely to the pressure force generated by its motion. Computations of such 'free-body' motions have been performed from two-dimensional solutions in the time domain by Adachi & Ohmatsu (1979) and Yeung (1982).

As in the analysis of other linear systems, Fourier synthesis provides a connection between the time and frequency domains. The damping and added mass can be derived indirectly as conjugate Fourier transforms of the impulse response. Alternatively, the impulse response can be evaluated as the inverse transform of either coefficient in the frequency domain. Indirect solutions of the free-body problem also can be based on Fourier analysis of the frequency-domain coefficients; this approach was initiated by Ursell (1964), and has been followed by Maskell & Ursell (1970) for a floating semicircle, and by Kotik & Lurye (1968) with an approximate analysis for a hemisphere.

Fourier analysis of transient experimental data has been proposed by Davis & Zarnick (1964), as an economical technique for measuring the motions of ship models in waves. This procedure has been applied by Ohmatsu (1980), but with limited accuracy at low frequencies. The present study illustrates the use of this technique in theoretical computations, by deriving the damping and added-mass coefficients of a floating body from Fourier transforms of the impulse-response function. It will be shown that this approach can be effective for an axisymmetric body, and the method which is employed can be extended to fully three-dimensional bodies of arbitrary shape. For complicated bodies which are described by a large number of discretized panels, this technique offers a theoretical advantage by reducing the computational burden of matrix analysis.

In the present work the three-dimensional floating-body problem is solved directly in the time domain to determine the impulse response of a circular cylinder with horizontal base, floating in water of infinite depth and moving parallel to the vertical axis. Green's theorem is used to obtain an integral equation for the velocity potential on the body surface. Integration of the Green function with respect to the angular coordinate yields a one-dimensional integral equation, with the singular element of the kernel expressed in terms of elliptic integrals. A Galerkin scheme is used to discretize the integral equation and Romberg quadratures are employed on each segment of the body. The body surface is replaced by a non-uniform grid of segments, concentrated near the corner. The solution is carried out in uniform time steps, with the velocity potential on the body obtained from a linear system of simultaneous algebraic equations.

The analytic basis for the problem is set forth in §2, followed in §3 by a study of the non-free-surface part of the solution and an evaluation of the two complementary limits for the added mass at zero and infinite time. (These correspond respectively to the limits of infinity and zero in the frequency domain, and by reflection to a double body in an unbounded fluid when the image moves either in phase with the lower half or in the opposite direction.) When the cylinder depth vanishes, classical results are recovered for the added mass of a thin circular disk. In the converse case, the added mass of a semi-infinite cylinder is derived by extrapolation.

The free-surface solution is developed in §4. The velocity potential obtained at each time step is integrated over the bottom of the cylinder to give a 'time-dependent added mass'. Numerical differentiation of this function with respect to time gives the pressure-force equivalent to the impulse-response function. Confirmation for the numerical results is demonstrated in §5 by comparing the Fourier transforms with the frequency-domain solution for the same body. The impulse-response function is used in §6 to study the free-body motions following an initial displacement or imposed velocity.

The possible advantages of using the impulse-response function as a practical computational tool for complicated three-dimensional body shapes are discussed in

§7. Unlike the analogous situation in the frequency domain, the coefficient matrix of the linear system which must be solved in the time domain is real, independent of free-surface effects, and can be inverted initially to reduce the computational burden at each time step. For fully three-dimensional vessels which must be represented by very large numbers of discrete panel elements, these differences imply a significant computational advantage for the time-domain approach.

2. Mathematical formulation

A right-circular cylinder with vertical axis floats in the free surface with its bottom at a depth D, as shown in figure 1. The fluid is unbounded in the domain beneath the free surface, exterior to the body. It is convenient to assume unit values for the cylinder radius, gravity, and the fluid density; hence the physical parameters of the problem are non-dimensionalized at the outset in terms of these three scales. Polar coordinates are used with the radial distance r measured from the vertical z-axis, $z = 0$ the plane of the free surface, and z positive upwards.

Starting from an initial state of rest at time $t = 0$, the body is forced to move vertically with a (non-dimensional) velocity $V(t)$ of small magnitude. The latter restriction justifies a linear theory. Notwithstanding this restriction, it can be assumed in the derivation that $V(t)$ is the unit step function, and the body acceleration is a delta function at $t = 0$. The resultant force exerted by the body on the fluid is referred to as the impulse-response function. More general vertical motions of the body can be analysed by linear superposition, or by convolution of the body acceleration and the impulse-response function.

Anticipating an axisymmetric flow, the velocity potential $\phi(r, z, t)$ is subject to Laplace's equation in the fluid domain, the free-surface boundary condition

$$\phi_{tt} + \phi_z = 0 \quad \text{on } z = 0, \tag{1}$$

and the body-surface boundary conditions

$$\phi_r = 0 \quad \text{on } r = 1, \quad -D < z < 0, \tag{2}$$

$$\phi_z = V(t) \quad \text{on } z = -D, \quad 0 \leqslant r < 1. \tag{3}$$

At large distances from the body the potential must vanish† for all finite times. Both the potential and its first time derivative must vanish on the free surface for $t \leqslant 0$.

Following Wehausen (1971), an integral equation for the velocity potential on the body surface can be derived from the time-dependent three-dimensional Green function $G(r, z, r', z', \theta, t)$, defined in the Appendix by (A 1). This Green function can be interpreted as the potential at the field point (r, z) due to a submerged source located at (r', z'), and depending also on the polar angle θ between r and r'. The source strength is a unit step function, jumping from zero to one at $t = 0$. If Green's theorem is applied to this function, with retarded time $(t-\tau)$, and to the time derivative of the velocity potential, the resulting integral equation for field points on the body surface S takes the form

$$2\pi\phi(r, z, t) + \int_0^t \mathrm{d}\tau \int_S \phi(r', z', t)\, G_{nt}(t-\tau)\, \mathrm{d}S + \int_S \phi(r', z', t)\, G_n(0)\, \mathrm{d}S = \int_{S_B} G(t)\, \mathrm{d}S. \tag{4}$$

† Like the Green function, the potential is $O(r^{-2})$ at large radial distances from the body. However it is sufficient in the problem statement to require boundedness at infinity (Stoker 1957, p. 191).

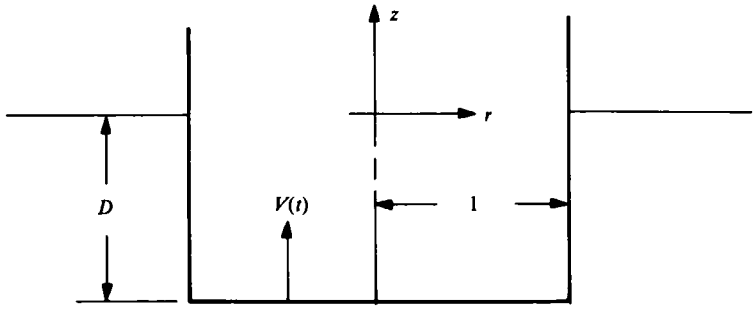

FIGURE 1. Sketch of cylinder in the azimuthal plane.

The normal derivatives of G in (4) are defined with respect to the source coordinates (r', z'). In the last term S_B denotes the bottom surface of the body where (3) applies. For clarity the spatial arguments of the Green function are not displayed.

Since the velocity potential is axisymmetric, the surface integrals in (4) can be integrated with respect to the angular coordinate, using results from the Appendix. This reduction yields line integrals along the trace C of the body surface in the (r, z) plane, with the Green function replaced by an axisymmetric ring source. Thus (4) is replaced by the one-dimensional integral equation

$$2\pi\phi(r,z,t)+\int_0^t \mathrm{d}\tau \int_C \phi(r',z',\tau)\, G_{nt}^{(F)}(t-\tau)\,\mathrm{d}l+\int_C \phi(r',z',t)\, G_n^{(0)}\,\mathrm{d}l = \int_{C_B} [G^{(0)}+G^{(F)}(t)]\,\mathrm{d}l. \quad (5)$$

Here (r, z) is on C, and C_B denotes the portion of C on the bottom of the cylinder. The differential element $\mathrm{d}l$ denotes $r'\,\mathrm{d}r'$ on the bottom, or $\mathrm{d}z'$ on the side of C. $G^{(0)}$ is the contribution from the Rankine source $1/R$ and its negative image above the free surface. This function and its normal derivative are expressed by (A 3–A 8) in terms of complete elliptic integrals which are logarithmically singular when the source and field points coincide. Since the remaining free-surface contribution $G^{(F)}$ vanishes when $t = 0$, $G^{(0)}$ represents the initial value of the total Green function.

Following the usual approach of boundary-integral methods, (5) is replaced by a linear system of algebraic equations corresponding to discrete segments of the body contour. For this purpose the contour C_B $(0 < r < 1;\ z = -D)$ is subdivided into N_B segments S_j $(j = 1, 2, \ldots, N_B)$ and the side $(r = 1;\ -D < Z < 0)$ into a similar set of N_S elements $(j = N_B+1, \ldots, N)$. The ensemble of $N = N_B+N_S$ segments is ordered in sequence starting at the cylinder axis, proceeding to the corner and then up to the free surface. The potential is assumed constant on each segment, with the value ϕ_j on S_j.

Invoking a Galerkin procedure, both sides of (5) are integrated over the segment S_i to yield the system of Volterra equations

$$\sum_{j=1}^{N} \left\{ A_{ij}^{(0)}\,\phi_j(t)+\int_0^t A_{ij}^{(F)}(t-\tau)\,\phi_j(\tau)\,\mathrm{d}\tau \right\} = \sum_{j=1}^{N_B} [B_{ij}^{(0)}+B_{ij}^{(F)}(t)]. \quad (6)$$

The four matrices in (6) are defined by

$$A_{ij}^{(0)} = s_i\,\delta_{ij}+\int_{S_i}\int_{S_j} G_n^{(0)}\,\mathrm{d}l_j\,\mathrm{d}l_i, \quad (7)$$

$$A_{ij}^{(F)}(t) = \int_{S_i}\int_{S_j} G_{nt}^{(F)}(t)\,\mathrm{d}l_j\,\mathrm{d}l_i, \tag{8}$$

$$B_{ij}^{(0)} = \int_{S_i}\int_{S_j} G^{(0)}\,\mathrm{d}l_j\,\mathrm{d}l_i, \tag{9}$$

$$B_{ij}^{(F)}(t) = \int_{S_i}\int_{S_j} G^{(F)}(t)\,\mathrm{d}l_j\,\mathrm{d}l_i, \tag{10}$$

δ_{ij} is the Kroenecker delta, and

$$s_i = 2\pi\int_{S_i}\mathrm{d}l_i \tag{11}$$

is the area spanned by the corresponding segment on S.

It is advantageous to use a finer subdivision of segments near the corner, since the solution is singular at this point, and also because the contribution to the hydrodynamic force from the pressure on the bottom increases in proportion to the radius. An appropriate choice is to use 'cosine spacing' on both the bottom and the side, with the segments on these two surfaces defined by the following end points:

$$r_j = \sin\left(\frac{\pi j}{2N_{\mathrm{B}}}\right) \quad (j = 0, 1, \ldots N_{\mathrm{B}}), \tag{12}$$

$$z_j = -D\cos\left(\frac{\pi(j-N_{\mathrm{B}})}{2N_{\mathrm{S}}}\right) \quad (j = N_{\mathrm{B}}, N_{\mathrm{B}}+1, \ldots, N). \tag{13}$$

After the total number N of segments is prescribed, usually as a power of two, the integer N_{B} is selected to minimize the discontinuity of segment length at the corner. With the segments defined by their end points in this manner, the area (11) of each segment is given by

$$s_j = \pi(r_j^2 - r_{j-1}^2) \quad (j = 1, 2, \ldots, N_{\mathrm{B}}), \tag{14}$$

$$s_j = 2\pi(z_j - z_{j-1}) \quad (j = N_{\mathrm{B}}+1, N_{\mathrm{B}}+2, \ldots, N). \tag{15}$$

3. The limits for $t = 0$ and infinity

Free-surface effects are absent in the limit $t = 0$. The integral equation (5) involves only the Green function $G^{(0)}$, the Rankine ring source and its negative image above the free surface. The discretized equation (6) simplifies to the form

$$\sum_{j=1}^{N} A_{ij}^{(0)}\,\phi_j(0) = \sum_{j=1}^{N_{\mathrm{B}}} B_{ij}^{(0)} \quad (i = 1, 2, \ldots, N), \tag{16}$$

where, after combining (7) and (9) with (A 3–A 8),

$$A_{ij}^{(0)} = s_i\delta_{ij} + \int_{S_i}\int_{S_j}\left\{\left(\frac{2}{\rho_+}(E-K)\,n_{r'} + \frac{4E}{\rho_+\rho_-^2}[(z-z')\,n_{z'} + (r-r')\,n_{r'}]\right) - (\hat{}\,)\right\}\mathrm{d}l_j\,\mathrm{d}l_i, \tag{17}$$

$$B_{ij}^{(0)} = \int_{S_i}\int_{S_j}\left\{\frac{4}{\rho_+}K(m) - \frac{4}{\hat{\rho}_+}K(\hat{m})\right\}\mathrm{d}l_j\,\mathrm{d}l_i. \tag{18}$$

Here (K, E) are the complete elliptic integrals with $\rho_\pm$ and the parameter m defined by (A 4–A 5). The symbol $\hat{}$ is used to denote image quantities above the free surface, with the sign of z' reversed, and $(\hat{}\,)$ denotes the image of all preceding terms in braces.

D	$M(0)$	$M(\infty)$
0.0625	1.4820	2.5887
0.125	1.5533	2.5371
0.25	1.6422	2.4652
0.5	1.7414	2.3775
1.0	1.8390	2.2859
2.0	1.9215	2.2057
4.0	1.9814	2.1467
8.0	2.0190	2.1091
∞	2.064	2.064

TABLE 1. Added-mass coefficients for cylinders of various depths D, in the limits $t = 0$ and $t = \infty$

To evaluate the matrices (17) and (18), polynomial approximations are used for the elliptic integrals (Abramowitz & Stegun 1964, equations 17.3.33–34), and Romberg quadratures for the numerical integration over each segment to a minimum absolute tolerance of 10^{-5}. Since $K(m)$ is logarithmically singular when m tends to unity, all contributions to the integrand of order $\log(1-m)$ or $(1-m)\log(1-m)$ are subtracted and integrated analytically. This special treatment of the logarithmic terms is made for all segments on the bottom or side if the corresponding term is singular at any point thereon. To the order indicated above the singular contributions in (17) and (18) are identical.

After solving (16) for the unknown vector $\phi_j(0)$, the added mass at $t = 0$ may be obtained by integration in the form

$$M(0) = \pi \int_0^1 \phi(r,0)\, r\, \mathrm{d}r = \frac{1}{2} \sum_{j=1}^{N_B} s_j \phi_j(0). \tag{19}$$

The results of this computation are given in table 1, and plotted in figure 2. Also included are the complementary results which follow in the limit $t = \infty$, defined more explicitly as the zero-frequency limit of the added-mass coefficient in the frequency domain. An alternative physical interpretation is in terms of a dilating double body in an infinite fluid, with the upper and lower ends moving in opposite directions. This complementary limit corresponds to a homogeneous Neumann condition on the free surface; the corresponding results are obtained simply by reversing the sign of the image terms in (17) and (18).

The added-mass coefficients listed in table 1 are derived from computations with 8, 16, 32 and 64 total segments on the body. In all cases the sequence is monotone decreasing as N increases. The convergence rate appears to be nearly quadratic. For example, with $D = 0.5$ the sequence for $M(0)$ is 1.7629, 1.7474, 1.7432, 1.7419. The entries in table 1 for finite values of D have been derived by Richardson extrapolation of each such sequence, and are believed to be accurate to at least three decimal places.

In the limit $D = 0$, the cylinder collapses onto a circular disk of unit radius in the plane $z = 0$. Analytical results are available from Lamb (1932, Section 102), with $M(0) = \frac{4}{3}$ and $M(\infty) = \frac{8}{3}$. (The latter value is derived by integrating the potential in Lamb's equation 11.)

The converse limit, $D \to \infty$, corresponds to the axial added mass of a semi-infinite cylinder. No analytical result is known for this case, but when the depth is large slender-body theory suggests that the effect from the opposite body end can be

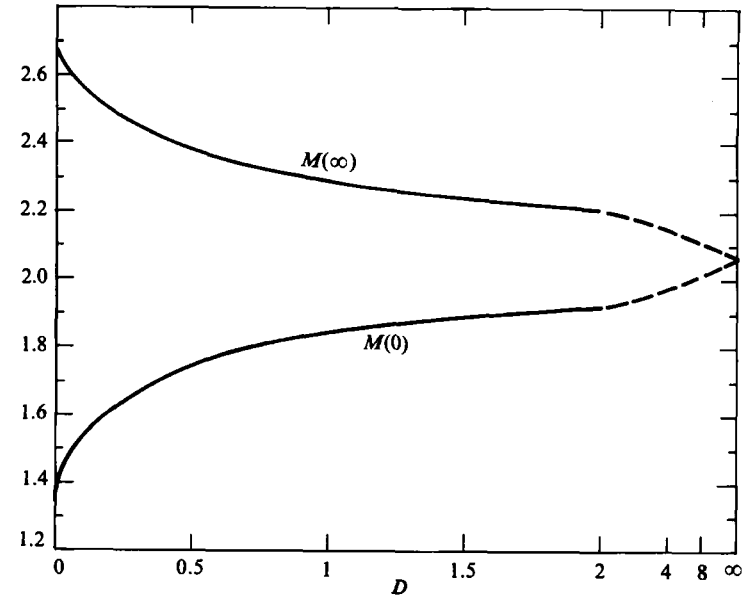

FIGURE 2. Added-mass coefficients in the limits of time equal to zero and infinity. Note that the abscissa is redefined to be inversely proportional to the depth D for $D > 2$, to display the asymptotic dependence in (20). The common limit of these two curves for $D = 0$ is the added mass from the end of a semi-infinite cylinder.

approximated by a point source equal in strength to the flux across that end, with a potential inversely proportional to the distance $2D$ (cf. Newman 1977). From this approximation it follows for $D \gg 1$ that

$$M \simeq C \pm \frac{\pi}{8D}, \quad t = \begin{pmatrix} \infty \\ 0 \end{pmatrix}, \tag{20}$$

where C is a constant and the sign (+ or −) corresponds to the image for $t = \infty$ or 0, respectively. Using (20) a numerical extrapolation may be performed separately from the two columns of data in table 1, with the common limit $C = 2.064$. This extrapolation is indicated by the broken curves in figure 2, which are plotted in the domain $D > 2$ with an inverse scale for the abscissa.

4. Solution of the free-surface problem

A uniform discretization in time reduces (6) to a linear system of algebraic equations which may be solved directly at each time step. Equivalently, the convolution integral in (6) may be evaluated by the trapezoidal rule, with the result

$$\sum_{j=1}^{N} \left\{ A_{ij}^{(0)} \phi_j(t_n) + \Delta \sum_{m=0}^{n-1}{}' A_{ij}^{(F)}(t_n - t_m) \phi_j(t_m) \right\} = \sum_{j=1}^{N_B} [B_{ij}^{(0)} + B_{ij}^{(F)}(t_n)]. \tag{21}$$

Here Δ denotes the time step, and $t_n = n\Delta$ is the time after the nth step. The primed summation sign denotes that the term $m = 0$ is multiplied by one half, corresponding to one end point of the trapezoidal rule.

Since the time derivative of (A 9) vanishes at $t = 0$, there is no contribution from (8) at the upper limit of the integral and no corresponding term with $m = n$ in (21). As a result, the only contribution to (21) from the new unknown vector $\phi_j(t_n)$ at each

time step is in the first term, where the coefficient matrix is independent of time and may be inverted at the outset. Thus the solution may be expressed explicitly in the form

$$\phi_k(t_n) = \sum_{i=1}^{N} [A_{ki}^{(0)}]^{-1} \left\{ \sum_{j=1}^{N_B} [B_{ij}^{(0)} + B_{ij}^{(F)}(t_n)] - \Delta \sum_{m=0}^{n-1}{}' A_{ij}^{(F)}(t_n - t_m)\, \phi_j(t_m) \right\}, \qquad (22)$$

where the first factor on the right side of this equation is the inverse of the matrix (17).

The first task in the numerical analysis of (22) involves computing the matrix (17), in the manner outlined in §3, and evaluating its inverse by Gauss elimination. (For a fully three-dimensional body, where N is substantially larger, decomposition of the coefficient matrix into lower- and upper-triangular matrices would be more effective at this stage.) Subsequently, for each time step, the time-dependent free-surface matrices (8) and (10) are evaluated in the manner described below. The remaining operations to evaluate the terms in braces in (22) are straightforward, and after carrying out the indicated matrix product the velocity potential for each segment is obtained at the new time step.

The evaluation of the time-dependent matrices (8) and (10) involves double integration of the free-surface Green function (A 9) and its derivatives. This is effected by reversing the order of integration and evaluating the double integrals over the pair of segments under the integral sign in (A 9). These integrals can be evaluated in closed form. The remaining single integral in (A 9) is evaluated by Romberg quadratures in unit steps of the variable $k^{\frac{1}{2}}$, with an absolute convergence requirement of 10^{-5} applied at each step.

If the matrix elements are stored for use at subsequent time steps the computational burden is linear for increasing time, except for the convolution summation over the index m which increases quadratically.

After each time step the velocity potential is integrated over the bottom surface in a similar manner to (19), to give the transient added-mass coefficient

$$M(t) \simeq \frac{1}{2} \sum_{j=1}^{N_B} s_j \phi_j(t). \qquad (23)$$

The term 'transient added mass' is analogous to the more conventional frequency-dependent added-mass coefficient $\mu(\omega)$ in the frequency domain. The pressure force acting on the fluid is the time derivative of (23), in accordance with the linearized Bernoulli equation. Since the body velocity is a step function, the pressure force is equivalent to the time derivative of the 'transient added momentum' equal to the product of the added mass and body velocity. Alternatively, $M(t)$ can be interpreted as the force due to a unit step-function acceleration of the body. This provides a more physical interpretation for the limit of (23) as $t \to \infty$. The definition (23) is consistent with the limits for $t = 0$ and infinity as defined in §3.

The impulse-response function can be evaluated as the derivative of (23) from the central-difference formula

$$L(t_n) \cong \frac{M(t_{n+1}) - M(t_{n-1})}{2\Delta}. \qquad (24)$$

Here the notation of Wehausen (1971) is adopted, with $L(t)$ the pressure force exerted by the body on the fluid following a delta-function acceleration from a state of rest.

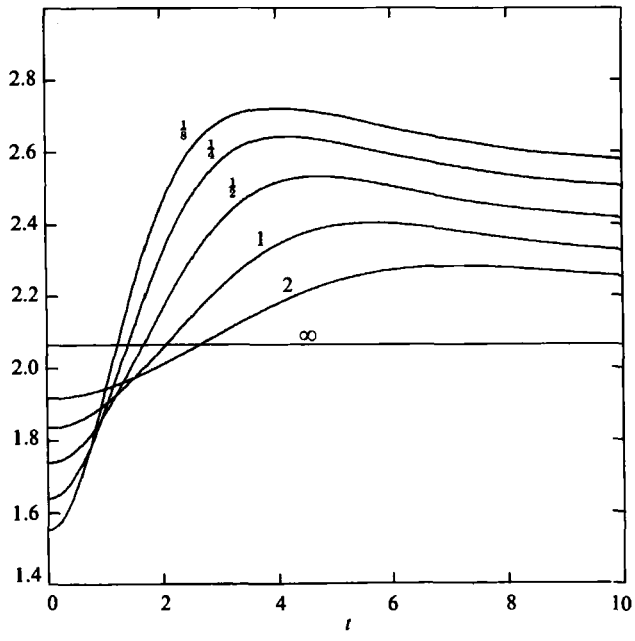

FIGURE 3. Transient added-mass coefficients for a family of cylinders with depths as shown.

More generally, for a time history with continuous acceleration $V'(t)$, the hydrodynamic pressure force is given by the convolution

$$F(t) = M(0)\, V'(t) + \int_0^t V'(t-\tau)\, L(\tau)\, \mathrm{d}\tau. \tag{25}$$

Computations of the transient added mass (23) and impulse-response function (24) are presented in figures 3 and 4 for several values of the cylinder depth D. The added mass increases from an initial value with zero slope at $t = 0$, reaches a single maximum, and then approaches the infinite-time limit from above. The impulse-response function increases linearly from zero at $t = 0$, reaches a maximum positive value before changing sign, and finally approaches zero from below as $t \to \infty$. Free-surface effects are diminished as D increases. The limit for $D = \infty$ is reproduced in figure 3 from table 1.

Asymptotic expansions can be derived by expressing the impulse-response function as the inverse sine transform of the damping coefficient (cf. (30) below). For small values of t, this transform can be expanded in a convergent power series with odd powers only, making use of the fact that the damping coefficient is exponentially small for high frequencies. (The latter bound requires $D > 0$.) By integration, $M(t)$ can be expanded in an analogous series with even powers of t. Thus the curves in figure 3 have zero slope at $t = 0$, and the impulse-response functions shown in figure 4 behave linearly near the origin.

For large values of t, the impulse-response function is related to the low-frequency asymptotic behaviour of the damping coefficient. Two terms in the latter expansion are easily derived by using the Haskind relations and the low-frequency approximation for the exciting force (Newman 1977, equations 6.169–173). After partial integration

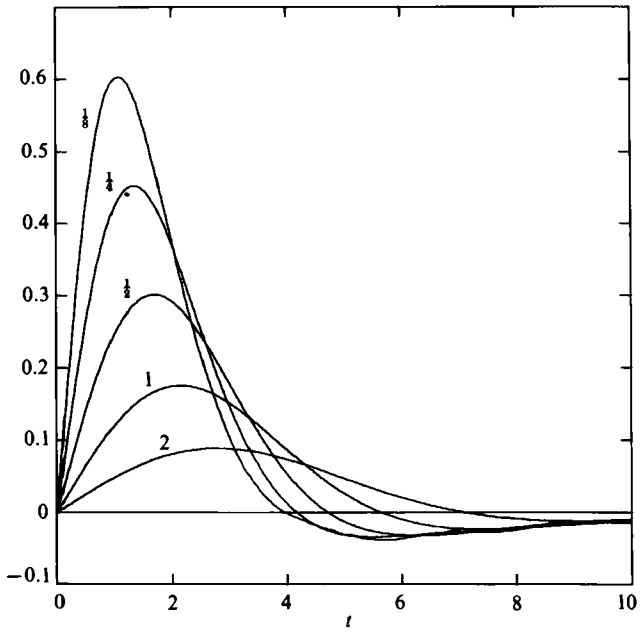

FIGURE 4. Impulse-response functions for a family of cylinders with depths as shown.

D	Amplitude	Period	T
0.125	0.0165	2.2	2.189
0.25	0.0058	3.0	2.972
0.5	0.0014	3.7	3.701

TABLE 2. Amplitude and period of the oscillatory error observed in computations of the impulse-response function with 16 segments. The last column shows the period of the lowest irregular frequency, computed from (28).

of the inverse sine transform it follows that

$$L(t) = -2\pi t^{-3} - [24\pi + 48m(\infty)]\, t^{-5} + o(t^{-5}), \tag{26}$$

where $M(\infty)$ is defined in §3. The maximum difference between this asymptotic approximation and the results plotted in figure 4 is 0.006 for $t > 7.1$ ($t > 8.3$ for $D = 2$). The leading term in (26) has been derived by Kotik & Lurye (1964).

Integration of (26) with respect to time gives the corresponding asymptotic expansion for the added-mass coefficient,

$$M(t) = M(\infty) + \pi t^{-2} + [6\pi + 12M(\infty)]\, t^{-4} + o(t^{-4}). \tag{27}$$

For small values of D, the numerical results for $L(t)$ and $M(t)$ contain a noticeable oscillatory component which persists for large values of time, contrary to (26) and (27). Table 2 shows the amplitude and period of these oscillations, for computations with 16 segments on the body. Tests with 32 segments indicate that this error is inversely proportional to the number of segments. The results plotted in figures 3 and 4 are based on linear extrapolation of the computations with 16 and 32 segments, to suppress the oscillatory error, but a small residual oscillation is perceptible for the

smallest depth ($D = 0.125$). A time step of 0.1 is utilized in these computations, and has been confirmed by tests with 0.05.

Table 2 indicates that the oscillatory component is roughly proportional to the inverse square of the depth D. This error can be related to the singular limit $D = 0$, where the right-hand side of (16) vanishes due to cancellation of the Rankine source and its image. Since the limiting solution of (16) is the velocity potential for the circular disk, the determinant of the coefficient matrix in (16) must be zero and the Fredholm determinant of (4) must vanish when the convolution integral is neglected. Thus the numerical procedure adopted here is ill-conditioned for small cylinder depths.

A striking agreement may be noted in table 2 between the observed period of the oscillatory error and the period of the first eigensolution for the interior domain of the body, subject to the linearized free-surface boundary condition and to a homogeneous Dirichlet boundary condition on the body surface. This interior eigensolution corresponds to the first 'irregular frequency' for solutions of the integral equation analogous to (4) in the frequency domain (cf. Ursell 1981). For the circular cylinder the wavenumbers of the axisymmetric eigensolutions are zeros of the Bessel function $J_0(k)$, and the irregular frequencies follow from the dispersion relation

$$\omega^2 = k \coth(kD). \tag{28}$$

The corresponding period $T = 2\pi/\omega$ is shown for the first zero, $k = 2.4048\ldots$, in the last column of table 2.

Adachi & Ohmatsu (1979) have considered the numerical solution of (4) in the time domain, and state that there is no effect on this solution from the irregular frequencies. (The opposite conclusion is reached by these authors when the transient problem is formulated in terms of a similar integral equation for the source strength on the body surface.) However, the proof of Adachi & Ohmatsu is based on orthogonality considerations which do not apply strictly to the discretized integral equation. Since the amplitude of the observed oscillatory error is proportional to the scale of discretization, it is possible to reconcile the present observations with the analysis of Adachi & Ohmatsu, and to conclude that there is indeed a connection between the irregular frequencies and the oscillatory error for large times in the impulse-response function.

5. Comparison with the frequency-domain solution

Following Wehausen (1971), the added-mass and damping coefficients for harmonic motion of the body with frequency ω can be expressed in terms of the impulse-response function by the Fourier transforms

$$\mu(\omega) = \mu(\infty) + \int_0^\infty L(t) \cos \omega t \, \mathrm{d}t \tag{29}$$

and

$$\lambda(\omega) = \omega \int_0^\infty L(t) \sin \omega t \, \mathrm{d}t. \tag{30}$$

Computations have been made for the circular cylinder $D = 0.5$, based on numerical integration of (29) and (30) using the trapezoidal rule with a time step of 0.1. The integrals are truncated at $t = 15$, and the subsequent contribution is estimated using (26) and the complex exponential integral. Various tests with smaller

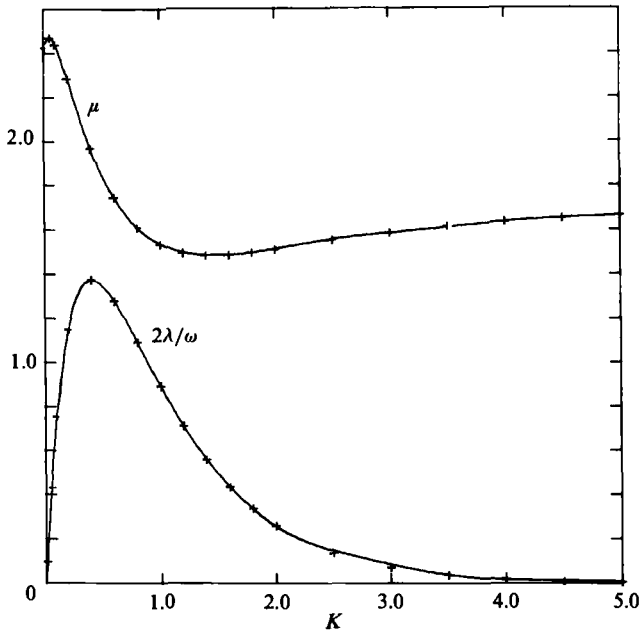

FIGURE 5. Damping and added-mass coefficients for the cylinder $D = 0.5$. Solid lines are computed from the Fourier transforms (29) and (30) of the impulse-response function. Symbols (+) denote the frequency-domain computations by Sclavounos (private communication) using a three-dimensional panel method.

time steps or Filon-type quadratures confirm the accuracy of this simple approach throughout the range of wavenumbers described below. Similarly, a comparison using 16 and 32 segments on the body surface reveals a maximum difference of 0.008, and suggests that 16 segments are sufficient to produce at least two decimals' accuracy in the added-mass and damping coefficients. There is no apparent non-uniformity in the vicinity of the irregular frequency.

The more accurate results with 32 segments are plotted in figure 5, as functions of the wavenumber $K = \omega^2$, based on the evaluation of (29) and (30) in wavenumber increments of 0.01. Assuming that the computational errors in these results are quadratic in the number of segments, the comparison indicated above implies an accuracy of the order of 0.002 for these computations.

Also shown in figure 5 are independent computations for the same cylinder, performed directly in the frequency domain with a three-dimensional panel code (Sclavounos, private communication). In the latter work a Galerkin approach is followed, and the cylinder is discretized in one quadrant with 2, 8, 32 and 128 flat panels. The added-mass and damping coefficients denoted in figure 5 by the symbols (+) are derived from the latter sequence by Richardson extrapolation. For values of K less than 2.0 the maximum differences relative to the time-domain results (solid curves) are 0.003 for the added-mass coefficient and 0.001 for the damping coefficient. The maximum differences for larger values of K are 0.006 and 0.007, respectively, at the wavenumbers 2.5 and 3.0 adjacent to the first irregular frequency ($K = 2.882$); it is expected that these larger differences are due to computational errors in the frequency-domain computations. Thus the expected accuracy of order 0.002 is confirmed in the computations based on the time-domain solution.

6. Response of a freely-floating cylinder

The vertical equation of motion for a floating body can be derived from its impulse-response function by adding the inertial and hydrostatic forces to (25). Thus, in the absence of an external force, the vertical displacement $y(t)$ satisfies the equation

$$[m+M(0)]\,y''(t)+Ay(t)+\int_0^t y''(t-\tau)\,L(\tau)\,\mathrm{d}\tau = 0, \tag{31}$$

where m is the mass of the body, and A is its waterplane area. Appropriate initial conditions must be specified for the displacement $y(0)$ and the velocity $y'(0)$.

Following the analogous two-dimensional study by Yeung (1982), two canonical problems are defined where: (1) $y(0) = 1$ while $y'(0) = 0$; and (2) $y(0) = 0$ while $y'(0) = 1$. In the first problem, where the response is denoted $y_1(t)$, the body is initially at rest in a position elevated from the state of hydrostatic equilibrium. In the second problem the response $y_2(t)$ results from initial conditions with the body in its equilibrium position, moving with a unit velocity. The latter condition implies a unit delta-function acceleration at $t = 0$, which must be added to the regular function $y_2''(t)$ to give the total acceleration.

If $y = y_1(t)$ is substituted in (31), and this equation is differentiated with respect to time, it follows that

$$[m+M(0)]\,y_1'''(t)+Ay_1'(t)+\int_0^t y_1'''(t-\tau)\,L(\tau)\,\mathrm{d}\tau+y_1''(0)\,L(t) = 0. \tag{32}$$

Alternatively, if $y = y_2(t)$ is substituted in (31),

$$[m+M(0)]\,y_2''(t)+Ay_2(t)+\int_0^t y_2''(t-\tau)\,L(\tau)\,\mathrm{d}\tau+L(t) = 0, \tag{33}$$

where the last term results from the acceleration at $t = 0$. Comparison of (32) and (33) and the initial conditions appropriate to each case yields the relation

$$y_2(t) = \frac{y_1'(t)}{y_1''(0)} = -\frac{y_1'(t)\,[m+M(0)]}{A}, \tag{34}$$

where (31) has been used to evaluate $y_1''(0)$. Yeung (1982) derives the same relation from a more complicated procedure involving the integral equation for the velocity potential. (In the two-dimensional case treated by Yeung the waterplane area A is replaced by the width of the body at the free surface.)

Numerical solutions of (31) may be developed from the impulse-response function evaluated in §4. Illustrative results are shown in figure 6 for the cylinder with depth $D = 0.5$. In the present units, $A = \pi$ and $m = AD = 0.5\pi$ in accordance with Archimedes' principle. The results shown for $y_1(t)$ and $y_2(t)$ are for non-dimensional times between 0 and 30, during which the cylinder performs approximately five cycles of a decaying oscillatory motion. Qualitatively similar figures have been presented for various two-dimensional bodies by Maskell & Ursell (1970) and Yeung (1982), and for the initial displacement of a floating hemisphere by Kotik & Lurye (1968). There is a weaker damping effect from the radiated waves in three dimensions, and thus a slower decay of the oscillatory motions.

For large values of time, Kotik & Lurye (1964) show by Fourier analysis that the displacement $y_1(t)$ has the asymptotic form

$$y_1 = \frac{6A}{\pi t^4} = 6t^{-4}, \tag{35}$$

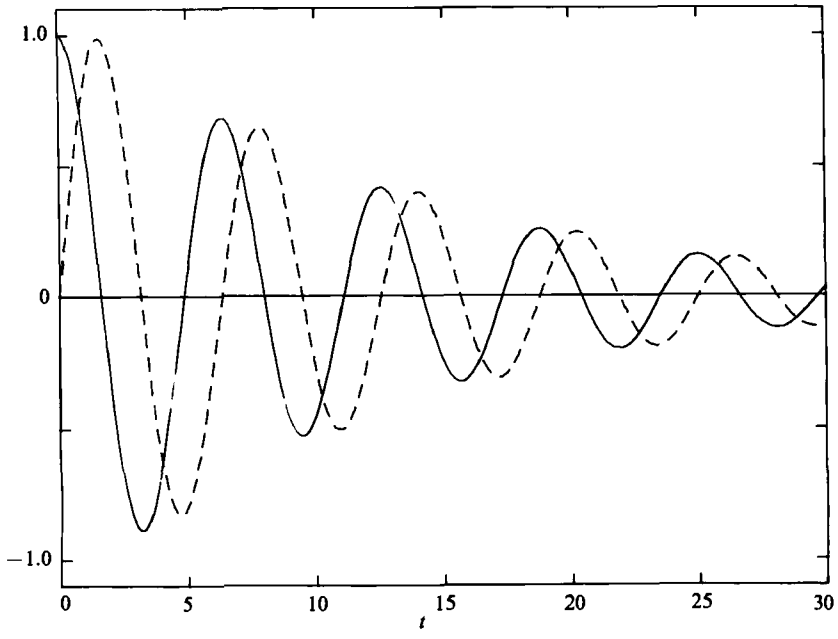

FIGURE 6. Free-body motions following an initial displacement (solid line) or initial velocity (broken line).

where the first result holds in general for a three-dimensional body. Analysis of the extinction rate in figure 6 indicates that this stage of the motion can be approximated by a harmonic function with amplitude $\exp(-0.08t)$. Thus there is an initial oscillatory state of motion with this amplitude, followed ultimately by the monotonic decay (35). Since these two amplitudes are comparable when $t \cong 250$, the total number of oscillatory cycles is apparently of the order of 40. This may be compared with the analogous estimate of nine cycles by Maskell & Ursell (1970) for the two-dimensional semicircular profile.

The results shown in figure 6 are computed from the impulse-response function described in §4, with 16 segments on the body and a time step of 0.1. A third-order Runge–Kutta method is employed to solve (31) with the same time step. Comparisons with 32 segments on the body show maximum differences in the third decimal place, and in the fourth decimal place for the maximum amplitude of each cycle. Separate computations of the functions y_1 and y_2 have been performed, and checked for consistency in accordance with (34).

7. Discussion

A computational procedure has been demonstrated for analysing the transient vertical motions of a floating axisymmetric cylinder. The same procedure may be applied to an axisymmetric body of arbitrary profile by using a more general geometrical discretization similar to that of Fernandes (1983). The analysis of axisymmetric bodies may be extended to other modes of motion where the angular dependence of the motion can be separated, provided a modified Green function is used corresponding to a ring source with the same angular dependence. In cases where

there is a non-zero normal body velocity at the free surface the numerical solution may be more complicated, with special care required to analyse the oscillatory behaviour of the Green function for large times.

If this method is to be useful in practice, the analogous diffraction force exerted on a fixed body by an impulsive wave also must be considered. Wehausen (1971) derives an appropriate extension of the Haskind relations to express the transient diffraction force in terms of the forced-motion velocity potential.

For fully three-dimensional bodies a two-dimensional integral equation must be solved with a discretization of the body in panels. It remains to show that this approach can be applied in the time domain, with sufficient numerical accuracy to provide reliable estimates of the relevant hydrodynamic forces, but no fundamental difficulty is expected.

Since Fourier transforms provide a simple relation between the time and frequency domains, it is appropriate to consider the possible advantages of each approach in the context of computations for practical three-dimensional vessels. In the frequency domain a complex system of linear equations is derived from the time-harmonic Green function and solved separately for each frequency. To account for wave effects in the damping and added-mass coefficients, the scale of geometric discretization on the body surface must be small relative to the wavelength. Special precautions are necessary in the vicinity of the irregular frequencies. This approach is well established and has been applied widely to the design of large offshore structures to predict their interactions with surface waves of moderate to long wavelengths. Typically such computations are performed using 100–500 panels, but current efforts in this field seek to extend N by an order of magnitude.

It is remarkable that the impulse-response function can be obtained by a time-stepping procedure with only one initial inversion of the real matrix (7). Since the solution of a linear system of equations requires $O(N^3)$ computations, this is the dominant computational burden if N is sufficiently large, and the possibility exists that the time-domain solution will be a more economical technique to utilize. The frequency-domain characteristics may be determined by direct computations at (say) 20 frequencies, or by Fourier analysis of the time-domain response at 200 time steps. Similar matrix techniques can be used in both cases to solve the respective systems of linear algebraic equations, with a computational burden proportional to the cube of the matrix dimension. If the same number of panels is used in each case, the (real) time-domain system can be solved in $\frac{1}{8}$th the time required for the (complex) frequency-domain system. Since the latter must be repeated for each frequency, there is a theoretical advantage of $\frac{1}{160}$ in favour of the time-domain approach. For this comparison to be relevant, N must exceed the number of time steps.

An additional advantage of the time-domain approach is that the damping and added-mass coefficients can be evaluated over a broad range of frequencies, without the need for a fine discretization of the body geometry commensurate with short wavelengths. Similarly, little or no concern is required with respect to the irregular frequencies. Indeed, the present results suggest that the magnitude of the large-time oscillatory error in the computed impulse-response function may provide a useful test of the adequacy of the discretization.

Financial support has been provided by the Office of Naval Research, Contract N0014-82-K-0198, and by the National Science Foundation, Grant MEA-8210649. I am indebted to Dr A. C. Fernandes, and Professors J. E. Kerwin, P. D. Sclavounos

and D. K. Yue for stimulating discussions and computational assistance. The calculations presented here have been performed on an IBM PC microcomputer equipped with a floating-point coprocessor.

Appendix. The Green function

The appropriate Green function in (4) can be derived from Wehausen & Laitone (1960, eq. 13.49) in the form

$$G(r, r', z, z', \theta, t) = \frac{1}{R} - \frac{1}{\hat{R}} + 2\int_0^\infty [1-\cos(k^{\frac{1}{2}}t)] \exp[k(z+z')] \times J_0(k(r^2+r'^2-2rr'\cos\theta)^{\frac{1}{2}})\,\mathrm{d}k, \quad (A\ 1)$$

where J_0 denotes the Bessel function of the first kind and

$$\left.\begin{matrix}\hat{R}\\ R\end{matrix}\right\} = [r^2+r'^2-2rr'\cos\theta+(z\pm z')^2]^{\frac{1}{2}}. \quad (A\ 2)$$

The corresponding 'ring source' is obtained by integrating (A 1) with respect to the angular coordinate θ. The result for the first term in (A 1) is the Rankine ring source,

$$\int_0^{2\pi} R^{-1}\,\mathrm{d}\theta = \left(\frac{4}{\rho_+}\right) K(m), \quad (A\ 3)$$

where the complete elliptic integral of the first kind $K(m)$ is defined by Abramowitz and Stegun (1964),

$$\rho_\pm = [(r\pm r')^2+(z-z')^2]^{\frac{1}{2}}, \quad (A\ 4)$$

and the parameter m is defined by

$$m = \frac{4rr'}{\rho_+^2} = \frac{1-\rho_-^2}{\rho_+^2}. \quad (A\ 5)$$

The normal derivative of (A 3) with respect to the source point is

$$\int_0^{2\pi} \left(\frac{\partial}{\partial n'}\right) R^{-1}\,\mathrm{d}\theta = \frac{4(z-z')}{\rho_+\rho_-^2} E n_{z'} + \left[\frac{4(r-r')}{\rho_+\rho_-^2}E + \frac{2}{\rho_+}(E-K)\right] n_{r'}, \quad (A\ 6)$$

where $E(m)$ is the complete elliptic integral of the second kind.

The image source given by the second term in (A 1) is treated in a similar manner, with the negative of the vertical source coordinate z' substituted throughout. The integral of the Bessel function in (A 1) is given by Watson (1952, equation 11.42(16)) and the complete expression for the free-surface ring source takes the form

$$\int_0^{2\pi} G\,\mathrm{d}\theta = G^{(0)}(r, r', z, z') + G^{(F)}(r, r', z, z', t), \quad (A\ 7)$$

where

$$G^{(0)} = \left(\frac{4}{\rho_+}\right) K(m) - \left(\frac{4}{\hat{\rho}_+}\right) K(\hat{m}), \quad (A\ 8)$$

and

$$G^{(F)}(t) = 4\pi\int_0^\infty [1-\cos(k^{\frac{1}{2}}t)] \exp[k(z+z')]\, J_0(kr)\, J_0(kr')\,\mathrm{d}k. \quad (A\ 9)$$

note that $G^{(F)}(t)$ and its first derivative both vanish at $t = 0$. The normal derivative

of (A 8) follows from (A 6), with the sign of z' changed in the image term, and the normal derivative of (A 9) can be evaluated under the integral sign using the relation $J_0' = -J_1$.

REFERENCES

ABRAMOWITZ, M. & STEGUN, I. A. 1964 *Handbook of Mathematical Functions*. Washington: Government Printing Office.

ADACHI, H. & OHMATSU, S. 1979 On the influence of irregular frequencies in the integral equation solutions to the time-dependent free surface problems. *J. Soc. Nav. Arch. Japan* **146**, 127–135.

DAVIS, M. C. & ZARNICK, E. E. 1964 Testing ship models in transient waves. In *Proc. 5th Symp. Naval Hydro.*, pp. 507–545. Washington: Government Printing Office.

FERNANDES, A. C. 1983 Analysis of an axisymmetric pneumatic buoy by reciprocity relations and a ring-source method. Ph.D. Thesis, MIT, Cambridge, Mass.

KOTIK, J. & LURYE, J. 1964 Some topics in the coupled theory of ship motions. In *Proc. 5th Symp. Naval Hydro.*, pp. 407–424. Washington: Government Printing Office.

KOTIK, J. & LURYE, J. 1968 Heave oscillations of a floating cylinder or sphere. *Schiffstechnik* **15**, 37–38.

LAMB, H. 1932 *Hydrodynamics*. Cambridge University Press.

MASKELL, S. J. & URSELL, F. 1970 The transient motion of a floating body. *J. Fluid Mech.* **44**, 303–313.

NEWMAN, J. N. 1977 *Marine Hydrodynamics*. Massachusetts Institute of Technology Press.

OHMATSU, S. 1980 Fourier transform of radiating wave by the impulse response of a floating body. *Trans. West Japan Soc. Nav. Arch.* no. 60, 65–75.

STOKER, J. J. 1957 *Water Waves*. Interscience.

URSELL, F. 1964 The decay of the free motion of a floating body. *J. Fluid Mech.* **19**, 305–319.

URSELL, F. 1981 Irregular frequencies and the motion of floating bodies. *J. Fluid Mech.* **105**, 143–156.

WATSON, G. N. 1944 *A treatise on the Theory of Bessel Functions*. Cambridge University Press.

WEHAUSEN, J. V. 1971 The motion of floating bodies. *Ann. Rev. Fluid Mech.* **3**, 237–268.

WEHAUSEN, J. V. & LAITONE, E. V. 1960 Surface waves. *Handbuch der Physik*, **9**, 446–778. Springer.

YEUNG, R. W. 1982 The transient heaving motion of floating cylinders. *J. Engng Maths* **16**, 97–119.